ADVANCED MATERIALS

Supporting Information

for *Adv. Mater.*, DOI: 10.1002/adma.201405207

Using Magnetic Levitation for Non-Destructive Quality Control of Plastic Parts

*Jonathan W. Hennek, Alex Nemiroski, Anand Bala Subramaniam, David K. Bwambok, Dian Yang, Daniel V. Harburg, Simon Tricard, Audrey K. Ellerbee, and George M. Whitesides**

Supporting Information for:

Using Magnetic Levitation for Non-destructive Quality Control of Plastic Parts

Jonathan W. Hennek[1], Alex Nemiroski[1], Anand Bala Subramaniam[1], David K. Bwambok[1], Dian Yang[2], Daniel V. Harburg[1], Simon Tricard[1], Audrey K. Ellerbee[1], and George M. Whitesides[1,3,4,*]

[1]Department of Chemistry and Chemical Biology, Harvard University,

12 Oxford St., Cambridge, MA 02138

[2]School of Engineering and Applied Sciences, Harvard University, 29 Oxford St., Cambridge, MA 02138

[3]Wyss Institute for Biologically Inspired Engineering, Harvard University,

60 Oxford St., Cambridge, MA 02138

[4]**Kavli Institute for Bionano Science & Technology,** Harvard University, 29 Oxford Street

Cambridge, MA 02138

	Common Name	IUPAC Name or Chemical Formula	$\rho_{Typical}$	Reference
			[g cm^{-3}]	
Plastics	PP	polypropylene	0.91-0.94	[1]
	LDPE	low-density polyethylene	0.92	[2]
	HDPE	high-density polyethylene	0.96	[2]
	PS	polystyrene	1.06-1.12	[1]
	Nylon 6	poly[imino(1-oxohexamethylene)]	1.14	[2]
	Nylon 6/6	poly[imino(1,6-dioxohexamethylene)iminohexamethylene]	1.14	[2]
	PMMA	polymethylmethacrylate	1.19	[1]
	PUR	polyurethane	1.2	[2]
	Bakelite	polyoxybenzylmethylenglycolanhydride	1.3	[1]
	PVC	polyvinyl chloride	1.39-1.42	[1]
	PET	polyethylene terephthalate	1.4	[2]
	POM	polyoxymethylene	1.41	[2]
	PTFE	polytetrafluoroethylene	2.28-2.30	[1]
Ceramics	Boron Nitride	BN	2.18	[1]
	Glass	SiO_2	2.40-2.80	[1]
	Boron Carbide	B_4C	2.5	[1]
	Aluminosilicate dihydrate	$Al_2O_3 \cdot SiO_2 \cdot 2H_2O$	2.59	[1]
	Cordierite	$Al_3(Mg,Fe)_2Si_5AlO_{18}$	2.66	[1]
	Beryllia	BeO	2.8	[1]
	Steatite	$MgSiO_3$	2.92	[3]
	Forsterite	Mg_2SiO_4	2.99	[3]
Other Materials	Amber		1.06-1.11	[1]
	Resin		1.07	[1]
	Gelatin		1.27	[1]
	Bone		1.70-2.00	[1]
	Clay		1.80-2.60	[1]
	Ivory		1.83-1.92	[1]
	Opal		2.2	[1]
	Marble		2.60-2.84	[1]

Table S1. List of materials with densities in the relevant range of MagLev.

Orientation of a heterogeneous object with cylindrical symmetry

We have previously shown that the height *h* and angle of orientation θ of an object in a linear magnetic gradient, and under the influence of gravity, are independent.[4] As such, to study the orientation of the object, we need only consider the angle-dependent part of the potential energy $U(\theta)$, which can be decomposed into a magnetic contribution $U_{mag}(\theta)$, and gravitational contribution $U_{grav}(\theta)$. As we have previously shown[4], in general, U_{mag} will depend on a competition between the lengths of the principal axes $(\lambda_u, \lambda_v, \lambda_w)$ of the object, where (u, v, w) are the body-fixed coordinates in the principal frame of reference of the object. Equation S1 defines the lengths of the principal axes $\lambda_l \in (\lambda_u, \lambda_v, \lambda_w)$ of the object in the body-fixed, principal frame of reference $(\hat{\mathbf{u}}, \hat{\mathbf{v}}, \hat{\mathbf{w}})$; we discuss these values in more depth in Subramaniam *et al*.[4]

$$\lambda_l{}^2 = \frac{\int_V \Delta\chi(l, v, w)\, l^2 dV}{\int_V \Delta\chi(l, v, w) dV} \tag{S1}$$

In general, the λ_l values determine the "size" of the object as seen by the magnetic field, and are therefore determined not just by the geometry of the object, but by the volume distribution of the relative magnetic susceptibility, $\Delta\chi$, as well. In this paper, however, we assume that differences in χ have a negligible effect on the orientation, and thus we assume that it is homogenous throughout the object, in which case the lengths of the principal axes are reduced to Equation S2.

$$\lambda_l{}^2 = \frac{1}{V}\int_V l^2 dV \tag{S1}$$

Here, the origin of a body-fixed principal frame of reference lies at the geometric center (centroid) of the object. For many common parts (such as a screw, washer, or rod with a square cross-section) the lengths of two principal axes of these moments will be degenerate. In this case, without loss of generality, we set $\lambda_u = \lambda_v$, and define the w-axis as the axis of rotational

symmetry of the object. For a rectangular rod with a square cross-section with side width W and length L, the volume is $V = W^2L$, the lengths of the principal axes are given in Eq. S1–S2.

$$\begin{aligned}\lambda_u{}^2 = \lambda_v{}^2 &= \frac{1}{V}\int_V w^2 dV = \frac{1}{W^2L}\int_{-W/2}^{W/2} u^2 du \int_{-W/2}^{W/2} dv \int_{-L/2}^{L/2} dw \\ &= \frac{1}{12} W^2 \end{aligned} \tag{S1}$$

$$\begin{aligned}\lambda_w{}^2 &= \frac{1}{V}\int_V w^2 dV = \frac{1}{W^2L}\int_{-W/2}^{W/2} du \int_{-W/2}^{W/2} dv \int_{-L/2}^{L/2} w^2 dw \\ &= \frac{1}{12} L^2 \end{aligned} \tag{S2}$$

Using the assumptions above, Equation S3 shows $U_{mag}(\theta)$ parameterized by the angle θ between the body-fixed w-axis and the MagLev x-axis.

$$\begin{aligned} U_{mag}(\theta) &= -\frac{2B_0{}^2\Delta\chi}{\mu_o d^2} V\left(\lambda_v{}^2 - \lambda_w{}^2\right)\sin^2\theta \\ &= -\frac{B_0{}^2\Delta\chi}{6\mu_o d^2} V(W^2 - L^2)\sin^2\theta \end{aligned} \tag{S3}$$

In this equation, V is the volume of the object. In the absence of any heterogeneity in density, $U_{mag}(\theta)$ is the only term that contributes a torque about the centroid of the object. For shapes with $W > L$ (e.g. washer), stable orientations occur at $\theta = 0°$ and $180°$. For shapes with $W < L$ (e.g. rod, screw), stable orientations occur at $\theta = 90°$ and $270°$. In general, the object orients to move as much of its volume away from the magnets.

For an object with heterogeneity in density $\rho_s(\vec{r}')$, the center of mass and centroid are not, in general, located at the same point. In these cases, gravity will impart an additional force on the center of mass of the object. The gravitational potential energy $U_{grav}(\theta)$ is defined in Equation S4.

$$U_{grav}(\theta) = -\overline{\rho}_s V g \mathbf{r}_{cm}{}' \cdot \hat{\mathbf{z}}' \tag{S4}$$

In this equation, $\overline{\rho}_s = \frac{1}{V}\int_V \rho_s(\vec{r}')dV$ is the volume-averaged density of the object, g is the acceleration due to gravity, $\mathbf{r}_{cm}{}'$ is location of the center of mass defined in the principal frame, and $\hat{\mathbf{z}}'$ is $\hat{\mathbf{z}}$ parameterized in the principal frame. For an arbitrary $\rho_s(\vec{r}')$, the coordinates of the $\vec{r}_{cm}{}'$ can be found by Equation (S5).

$$\vec{r}_{cm}{}' = \frac{1}{\overline{\rho}_s V}\int_V \vec{r}'\rho(\vec{r}')\, dV \tag{S5}$$

We consider a simple case where defects occur along the principal w-axis such that $\vec{r}_{cm}{}' = (0, 0, w_{cm})$. In particular, we define a small cubic inclusion with density ρ_i, side length l, volume $V_i = l^3$, and displacement z_i along the w-axis of a rod of density ρ_r. In this case, the center for mass is

$$\begin{aligned} w_{cm} &= \frac{1}{\overline{\rho}_s V}\left[\int_{V_r} w\rho_r\, dV - \int_{V_i} w\rho_r\, dV + \int_{V_i} w\rho_i\, dV\right] \\ &= \frac{1}{\overline{\rho}_s V}\left[\rho_r W^2 \int_{-\frac{L}{2}}^{\frac{L}{2}} w dw - \rho_r l^2 \int_{z_i-\frac{l}{2}}^{z_i+\frac{l}{2}} w dw + \rho_i l^2 \int_{z_i-\frac{l}{2}}^{z_i+\frac{l}{2}} w dw\right] \\ &= -\frac{1}{\overline{\rho}_s V}(\rho_i - \rho_r)V_i z_i \end{aligned} \tag{S5}$$

In the body-fixed frame of reference, $\hat{\mathbf{z}}' = (0, \sin\theta, \cos\theta)$, and therefore $\mathbf{r}'_{cm} \cdot \hat{\mathbf{z}}' = w_{cm}\cos\theta$ and $U_{grav}(\theta) = -\overline{\rho}_s V g\, w_{cm}\cos\theta$. After substituting Equation S5 for w_{cm}, Equation S6 shows the total potential energy of the object in MagLev.

$$U(\theta) = -\frac{{B_0}^2 \Delta\chi}{6\mu_o d^2} V(W^2 - L^2)\sin^2\theta\ - (\rho_i - \rho_r)V_i g z_i\ \cos\theta \tag{S6}$$

For the calculations shown in Figure 3, we use the magnetic field B_0 = 0.385 T measured at the surface of the pair of 2” x 2” x 4” magnets separated by d = 4.5 cm. For the rod with

L = 2.5 cm and W = 1 cm, we have $V = W^2L = 2.5\ \text{cm}^3$ and $W^2 - L^2 = -5.25\ \text{cm}^2$. In Figure 3, we find the equilibrium orientation by minimizing $U(\theta)$ with respect to θ for a range of V_i, z_i, and $\Delta\chi$.

To get an intuitive sense of the behavior of objects in this potential well, we normalize the coefficients and extract a general form of the potential energy $U(\theta) = -[\sin^2\theta + A\ \cos\theta]$. In the main text, we measure the angle of inclination $\alpha = 90^\circ - \theta$ from the y-axis (for experimental simplicity); making the substitution we arrive at $U(\alpha) = -[\cos^2\alpha + A\ \sin\alpha]$. In Figure S1, we show how the minimum value of $U(\alpha)$ changes with the relative strength of the magnetic and gravitational contributions (changing value of A).

Use of Rectangular Magnets

For a square magnet and objects that are small relative to the length of the magnet, the object will be free to rotate around the z-axis because of the approximately cylindrically symmetric magnetic field near the z-axis. This random rotation can complicate experimental measurements. To simplify measurements and analysis, we used rectangular magnets and oriented them with the narrower dimension along the x-axis and the wider dimension along the y-axis. Using this configuration increased the magnetic confinement along the x-axis and decreased the confinement along the y-axis (relative to square magnets), thereby breaking the cylindrical symmetry of the magnetic field and constraining the w-axis of the rods to lie in the y-z plane. Furthermore, because ${B_y}^2 \ll {B_z}^2$ in this configuration, the contribution to the energy from B_y can be ignored: in our model, we only consider the effect of B_z.

Figure S1. Schematic depicting the orientation of levitation for a rod with a square cross section having density ρ_r. When the length L of the rod is < the width W (A), the rods w-axis will orient towards $\theta_0 = 0^\circ$ or 180° (L along z-axis). When L > W (B), the rods w-axis will orient towards $\theta_0 = 90^\circ$ or 270° (L along y-axis). If an inclusion with density ρ_i, volume v_i, and position along the w-axis w_i is introduced (C), the rod will levitation at an angle $\alpha = 0$ when $\rho_i = \rho_r$ (D), $\alpha > 0$ when $\rho_i < \rho_r$ (E), and $\alpha < 0$ when $\rho_i > \rho_r$ (F).

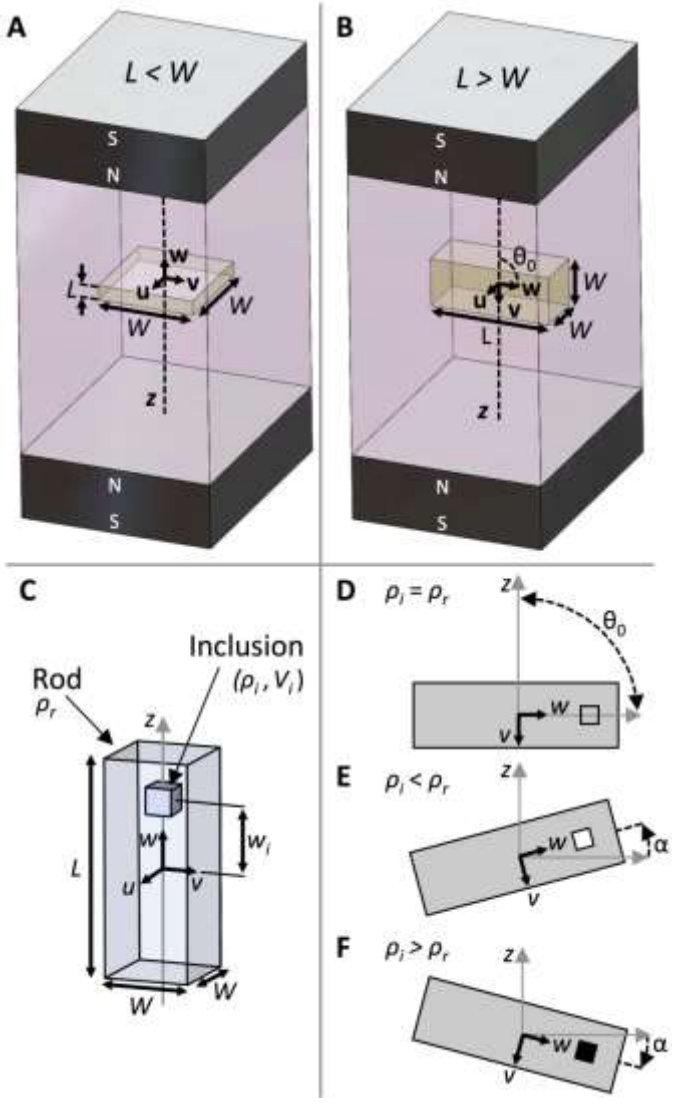

Figure S2. Plot of $U(\alpha)$ for various values of *A*. The red arrows show the minimum value α_{min}, where the object will attain a stable equilibrium for each given *A*. (Inset) Plot of the calculated α_{min} vs. A.

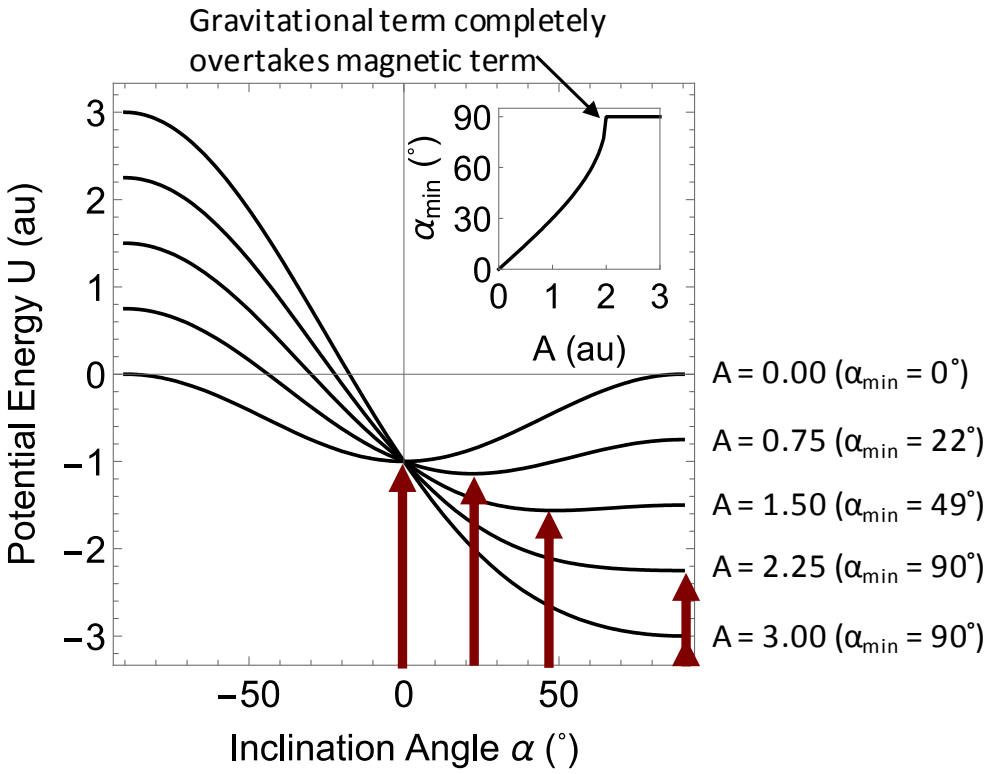

Micro-CT Analysis of Nylon Washers

Micro-CT analysis was performed using a X-Tek HMXST225 tomography system with x-ray voltage and current set to 70 kV and 102 µA, respectively. Data were analyzed using the VGStudio MAX software suite using following steps: 1) surface determination was performed on the objects with "remove small particles and voids" selected (note: if this step was not selected, the subsequent steps required ~40 hours of computation time), 2) a region of interest was selected to remove the sample holder and surrounding air, and 3) defect detection was performed using the porosity/inclusion module (probability threshold > 1, minimum volume = 8 voxel, maximum volume = 5 mm^3). Resulting images were modified using Adobe Photoshop to improve the contrast between the plastic parts and the small colored defects.

3D-Printed Model Rods

Model rods were printed using a Stratasys Objet30 Pro desktop three-dimensional (3D) printer based on drawings produced with Solidworks computer aided design software. The body of the rods was composed of Objet Veroblue RGD 840, a polyacrylate, and inclusions were made from printer support material, a polyacrylate with a lower degree of cross-linking. The density of a pristine rod and an inclusion were determined by levitating the object in 1.0 M $MnCl_2$ in the MagLev configuration described in the main text, measuring the height of levitation, and comparing the height to standards of known density (American Density Materials, Inc.). A linear magnetic field gradient was assumed.

Figure S3. Modeled levitation angle α for polyacrylate rods having ρ = 1.184 g/cm^3 containing a single void (air, ρ = 0.001 g/cm^3) of different volumes. Values are calculated for the same experimental conditions as used in Figure 3a (void = 10 mm from centroid, [$MnCl_2$] = 0.05 M). The largest inclusion volume is only 0.06% of the total volume of the 2.5 x 1 x 1 cm rod. The sensitivity of MagLev is, therefore, quite high when the Δρ between the majority material and the defect is high.

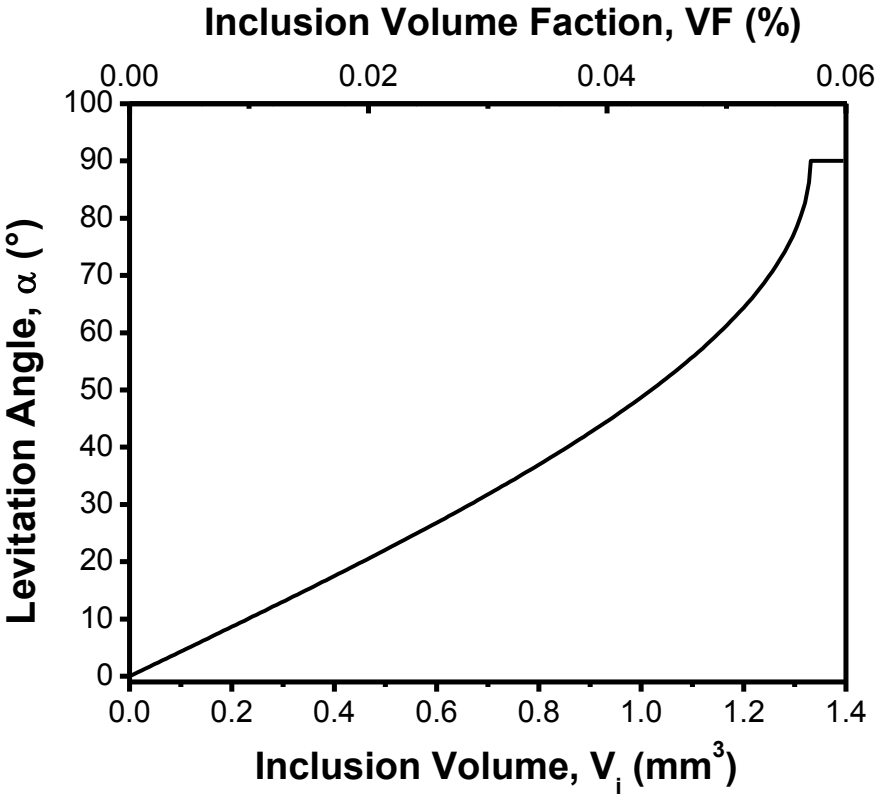

Exposure of Nylon 6/6 Objects to Simulated Harsh Environmental Conditions

We selected seven 3-cm Nylon 6/6 rods, exposed half of each rod to UV light (100 W), and measured α of the rods at 12-hour intervals for 72 hours. Figure S3 shows the α of the rods versus illumination time when levitating in an aqueous solution containing 0.075 M $MnCl_2$ + 1.26 M $ZnCl_2$. At t = 0, a negative α was observed in some cases because the portion of the rod exposed to UV light was chosen at random and α was measured as a deviation above the horizon for the exposed side.

We exposed half of several 3-cm Nylon 6/6 rods to deionized water, sea water (0.60 M NaCl), and a dilute acidic solution (0.10 M HCl) all at 50 °C for 24 hours to characterize the ability of MagLev to detect structural changes in plastic parts after exposure to harsh environments. Rods were placed in an aqueous solution of 0.10 M $MnCl_2$ + 1.26 M $ZnCl_2$ and levitated in a MagLev device (Figure S4). In all cases the exposure to degrading environments leads to a decrease in density of the exposed region.

We mimicked local thermal stress on an object by placing a small metal nut onto the end of a Nylon 6/6 screw and then putting the thermally conductive metal in contact with a hotplate set to 150 °C for 30 minutes. While thermal degradation of Nylon 6/6 typically results in a yellow discoloration, the small area of the exposed region made any potential discoloration undetectable by eye. The screws were then submerged in aqueous solutions of 0.10 M $MnCl_2$ + 1.26 M $ZnCl_2$, placed into the MagLev device, and photographed (Figure S5). The screw tilt angle with respect to the bottom magnet face was measured using ImageJ. As shown in Figure S5, thermal stress decreases the density of Nylon 6/6. The local change in density is detectable by MagLev as seen by an orientation deviation from horizontal.

Figure S4. Levitation angle, α, as a function of time for 3 cm Nylon 6/6 rods after half of the rod was exposed to a 100 Watt UV-light for a total of 72 hours (n = 7). Rods were levitated in an aqueous solution containing 0.075 M $MnCl_2$ + 1.26 M $ZnCl_2$.

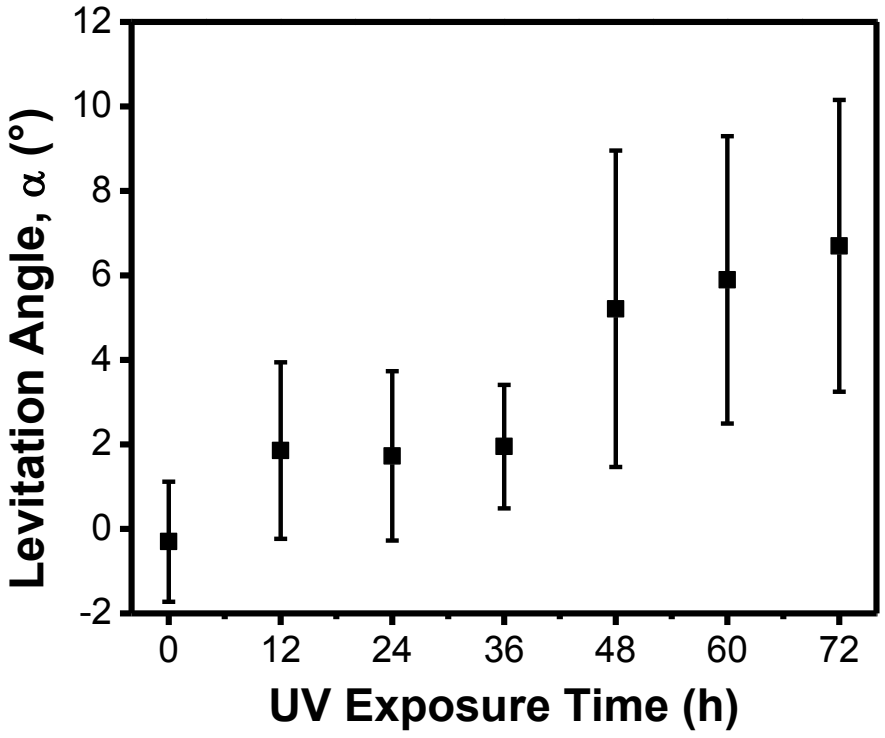

Figure S5. Photographs of Nylon 6/6 rods half of which were exposed to a variety of environmental conditions known to degrade the physical properties of plastics levitating in an aqueous solution of 0.10 M $MnCl_2$ + 1.26 M $ZnCl_2$. Rods were exposed to various degrading environmental conditions at 50 °C for 24 hours. The use of rectangular prism magnets (2.5 x 2.5 x 10 cm) confines the rods along the y-z plane. The pristine rod levitates horizontally to the face of the magnet while the other rods levitate with a deviation ranging from 10-15°, depending on the conditions. In all cases, exposure to degrading environments leads to a decrease in the density of the exposed region. The exposed area is the left half of the rods in the photographs.

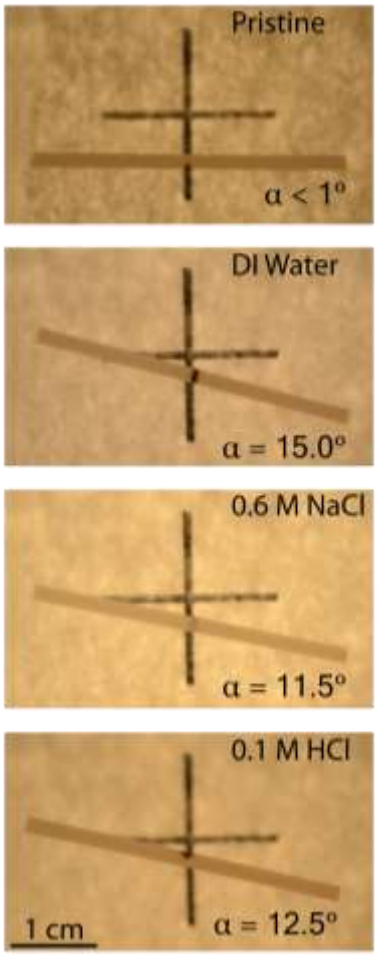

Figure S6. Photographs showing Nylon 6/6 screws levitating in an aqueous solution of 0.10 M $MnCl_2$ + 1.20 M $ZnCl_2$ with rectangular prism magnets (2.5 x 2.5 x 10 cm) placed 5.5 cm apart. A pristine screw (A) levitates with a tilt angle relative to the bottom magnet face of 0°. When screws were subjected to local thermal stress in the highlighted area for 30 minutes at 150 °C, a reduction in density in the affected area causes the screw to tilt with the lower density portion oriented upwards.

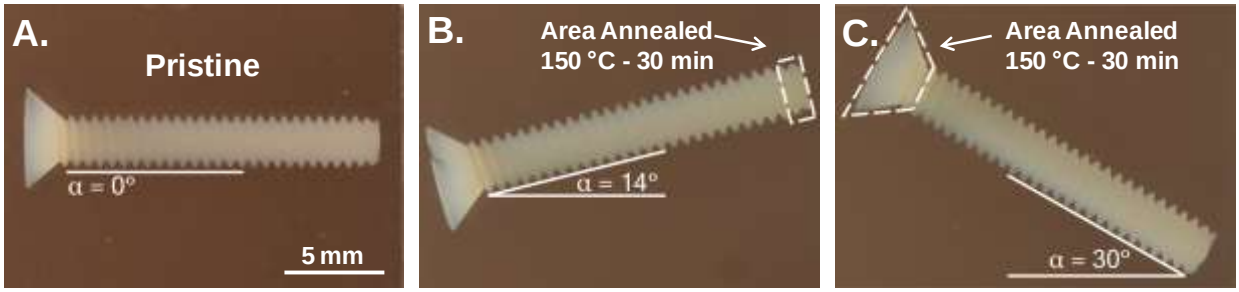

Counterfeit Rulon Detection

We tested real and fake Rulon® J using the same method as described for Rulon® 641. The paramagnetic solution used was 0.24 M $MnCl_2$ in 48% water, 52% Heavy Liquid (GEOLiquids Inc.) having a density of 1.9776 g/cm^3. Seven real and fake sleeve bearings were levitated at the same time and their heights were recorded. Figure S6 shows a box plot of the levitation height of each type. We found for real Rulon® J an $h_{avg} = 2.60 \pm 0.68$ cm ($\rho_{avg} = 1.97 \pm 0.01$ g/cm^3) and for fake Rulon® J an $h_{avg} = 1.16 \pm 0.44$ cm ($\rho_{avg} = 1.99 \pm 0.01$ g/cm^3) corresponding to a p-value of 7.24×10^{-4}.

We also tested Rulon® LR and found that real Rulon® LR is slightly magnetic (presumably ferromagnetic, as a result of metal oxide additives). When the paramagnetic solution was matched to approximately the density of the Rulon® LR bearing and placed in a MagLev device, the bearing was attracted to either the top or the bottom magnet. We found the magnetism of Rulon® LR to be small; a NdFeB magnet with a surface field of 0.4 T is not strong enough to attract the part in air. The fake Rulon® LR samples we tested, on the other hand, were not magnetic and levitated in a 0.50 M $MnCl_2$ (in 30/70 water/Heavy Liquid). Images of real and fake Rulon® LR are shown in Figure S7.

Figure S7. Box plot showing levitation height for real and fake Rulon® J (n = 7) levitating at the same time in 0.24 M $MnCl_2$ 48:52 water:Heavy Liquid mixture.

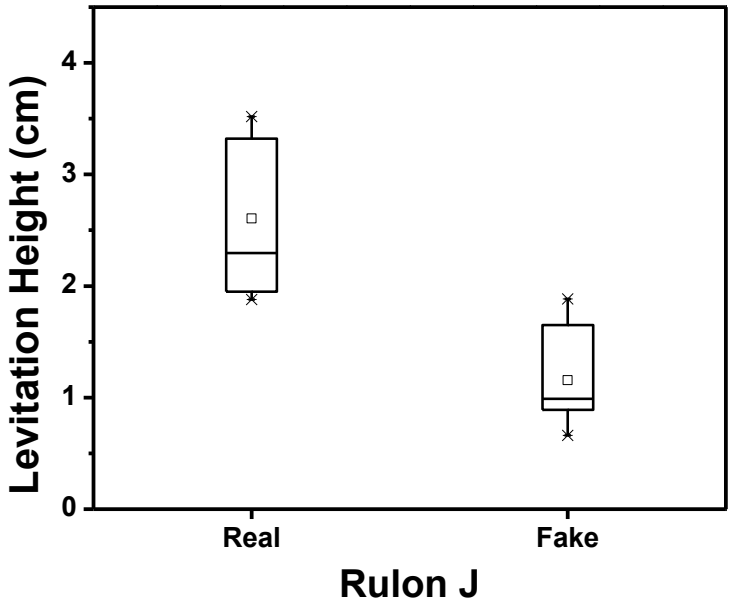

Figure S8. Images of stable levitation positions of real and fake Rulon® LR. The fake Rulon® consistently levitates at ~2.0 cm whereas the real Rulon® LR is attracted to either the top or bottom magnet and does not levitate in the solution. Images are cropped and put side by side for clarity.

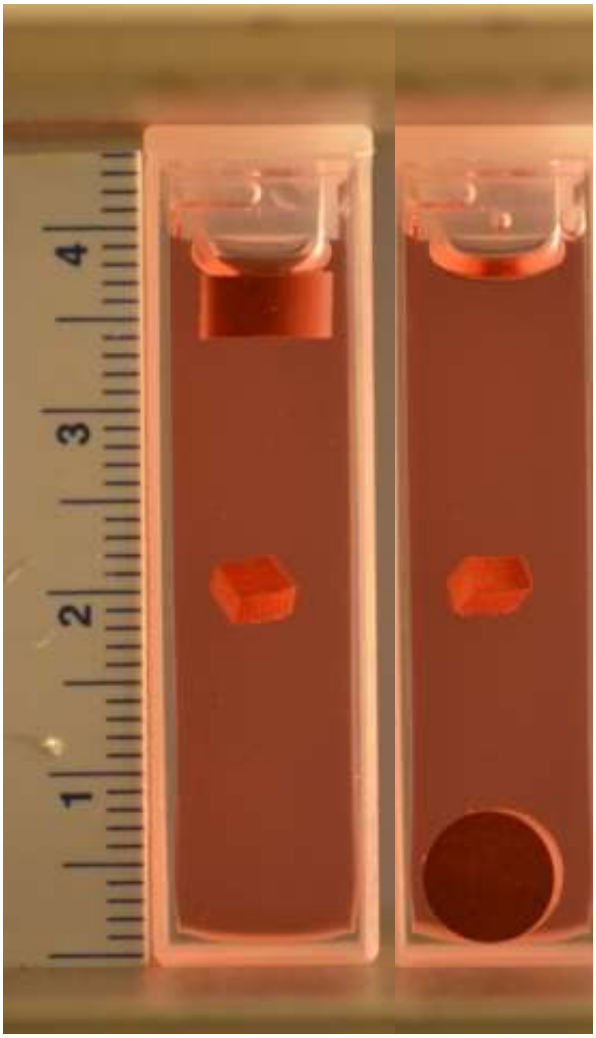

REFERENCES

[1] W. M. Haynes, *CRC Handbook of Chemistry and Physics (95th Edition)*, CRC Press, **2014**.

[2] G. W. Ehrenstein, *Polymeric Materials: Structure, Properties, Applications*, Hanser Publishers, **2001**.

[3] N. Soga, O. L. Anderson, *J. Am. Ceram. Soc.* **1967**, *50*, 239.

[4] A. B. Subramaniam, D. Yang, H.-D. Yu, A. Nemiroski, S. Tricard, A. K. Ellerbee, S. Soh, G. M. Whitesides, *Proc. Natl. Acad. Sci. U. S. A.* **2014**, *111*, 12980.